The 15th International Conference on Wind Engineering
Beijing, China; September 1-6, 2019

Mixture model approach for peak factor estimation and its application in cladding design

F. Rigo[a,b], T. Andrianne[a], V. Denoël[c]

[a]*Wind Tunnel Lab, University of Liège, Belgium*
[b]*FRS-FNRS, National Fund for Scientific Research, Belgium*
[c]*Structural & Stochastic Dynamics, University of Liège, Belgium*

ABSTRACT: To design reliable structures, extreme pressures and peak factors are required. In many applications of Wind Engineering, their statistical analysis has to be performed by considering their non-Gaussian nature. In particular, in the shear layers and where local vortices are formed, it is commonly observed that measured pressures might exhibit two or more significant components, which can be modeled with mixture models. Mixing two components with unequal weight may result in much larger non-Gaussianities (even if the two components are Gaussian) than a single (non-Gaussian) component. For this reason and some others, it is important to split a mixed flow into its underlying components [1]. In this paper, we propose a novel de-mixing method. Unlike existing approaches which are based on a nonlinear least-square fitting of the probability density function (PDF), the proposed method is supported by the different timescales of the mixed phenomena. The method is briefly described, and two examples of application are given.

KEYWORDS: wind pressure · peak factor · non-Gaussianity · mixture distribution · wind tunnel tests · low-rise building · monotone criterion

1 INTRODUCTION

This work focuses on the statistical analysis of wind pressures, involving significant non-Gaussianity, in the scope of building roofs. Peak factor estimation is necessary for the prediction of wind loads and thus the design of structures. The design of cladding and other facade elements with respect to the local minimum pressures is a major aim of structural design.,

The precision of wind tunnel measurements is necessary to keep important information: high sampling frequency, fine tap spatial distribution, long samples. With the increasing of pressure sensors precision in terms of sampling frequency, local effects can be better captured. However, the question can be raised about the relevance of very local effects, negligible in term of spatial and time scale compared to the entire structure. Amerio *et al.* [2] reported pressure coeffcients as low as -14 and Lin *et al.* [3] until -18 near roof corners of flat roof low buildings.

Many research works have been carried about the non-Gaussian statistics analysis of wind pressure [4, 5, 6, 7, 8]. Their purpose is to estimate peak factors, based on the translation process [9]. Peak factor can be estimated using the Hermite moment-based model [10] applied to the Gaussian peak factor of the classical peak factor model [11]. This Hermite moment-based approach relies on a transformation of a Gaussian into a non-Gaussian softening process (cubic translation) [7]. For many wind pressures, there is a good correlation between the peak factor g and high-order statistics (skewness γ_3 and kurtosis γ_4).

There exist also more advanced models, such as the modified Hermite model [12] or the revised Hermite model [13] which are able to deal with stronger non-Gaussianity. The former is quite heavier to solve due to a non-linear system; the latter requires conditions on γ_3 and γ_4. However, the Hermite moment-based model is less precise when pressures are significantly non-Gaussian. The cubic translation model requires the process to satisfy the monotone condition [14]. Peng [15] proposes a mapping of statistics in the (γ_3, γ_4) plane to reach the monotone condition by adjusting their value but the physical interpretation is less easy. Another kind of solution is a point-to-point distribution function mapping between Gaussian and non-Gaussian processes, assuming a Weibull or Gamma distribution [2]. This model allows to obtain an analytical evaluation of the peak factor but only in the case of a Weibull or Gamma distribution and is not general enough to handle multiple mode distributions.

Indeed, wind pressure on a low-rise building roof can be highly non-Gaussian and typically features two distinct and interacting phenomena. In worst cases (of large non-Gaussianity), the pressure distribution can even become bimodal which immediately calls for a separation of the two different phenomena and modes: e.g. the turbulent background and a component linked to the main flow behavior (corner vortices). By studying the probability density function (PDF), such modes can be highlighted. Traditional peak factor models, such as the cubic translation model [10] fail to predict peaks of the mixed process, but are much more accurate as soon as the tail component only is considered. The PDF is however a low rank statistical property and part of information is lost. The analysis is thus performed together with higher rank properties such as the autocorrelation, observing that the timescales associated with the two mixed components are different: (i) the slow turbulent flow and (ii) the fast shedding/flapping of corner vortices flow. We present a de-mixing operation based on the PDF and autocorrelation, making it possible to select the process of interest in the tail of the distribution and to restore the good agreement between g and (γ_3, γ_4) by satisfying the monotone condition. This is the option that is followed in our study.

The main contribution of the paper is to propose a solution for the treatment of significantly non-Gaussian pressure processes, thanks to a new way to separate the different contributions in the wind flow and to estimate peak factors based on long time wind pressure measurements. This paper first summarizes the algorithm for pointwise pressure data de-mixing based on the PDF and the autocorrelation [16]. High-order and rank statistics are studied, and instead of adjusting skewness and kurtosis through mapping, we suggest dealing with these processes by first de-mixing the wind pressure process, and then applying a cubic translation model to the tail component. By doing so, the peak factor predicted by the model (after de-mixing) is not only computable with the model but also in much better agreement with the peak factor obtained with statistical treatment of long data series. The general methodology that is proposed to decompose the wind pressure. The developed methodology will be illustrated with the analysis of wind pressure measurement on a square low-rise building flat roof, with a 45° wind orientation but can be applied to other practical cases of wind around buildings that require an estimate of wind loads on areas. After understanding the kind of flow involved and basic pressure statistics, the de-mixing methodology is explained. Then, processes with bimodal distributions are simulated to deduce statistical parameters violating the monotone condition. A parallel between autocorrelation and probability distribution decomposition is applied to decompose the pressure into simple components. Finally, it is shown that usual peak factor formulations are sufficiently accurate to model extreme values and their application in cladding design is discussed.

2 METHODOLOGY

2.1 *Cubic translation and peak factor estimation*

A usual way to estimate peak factors from pressure measurement uses cubic translation from a Gaussian process u to a non-Gaussian (softening) one x [10], and the Hermite moment-based model:

$$x = \kappa \left[u + \sum_{n=3}^{\infty} h_n H_{n-1}(u) \right] \approx \kappa \left[u + h_3 \left(u^2 - 1\right) + h_4 \left(u^3 - 3u\right) \right] \tag{1}$$

where κ is a scale factor that ensures x has unit variance and H_n is the n^{th} Hermite polynomial. A softening process is characterized by a wider tail in the distribution compared to a Gaussian one (*i.e.* with $\gamma_e = \gamma_4 - 3 > 0$). Most of wind pressure measured on buildings and roofs are softening processes. The mean peak factor is computed by Kareem *et al.* [4],

$$\mu_{g_{Her}} = \kappa \left\{ \left(\beta + \frac{\gamma}{\beta} \right) + h_3 \left[\beta^2 + 2\gamma - 1 + \frac{1.98}{\beta^2} \right] + h_4 \left[\beta^3 + 3\beta(\gamma - 1) + \frac{3}{\beta} \left(\frac{\pi^2}{6} - \gamma + \gamma^2 \right) + \frac{5.44}{\beta^3} \right] \right\} \tag{2}$$

where h_3, h_4, κ are coefficients of moment-based Hermite model [7], the Euler's constant is $\gamma \approx 0.5772$, and

$$\begin{gathered} \beta = \sqrt{2\ln(\nu_0 T)}, \quad \nu_0 = \sqrt{\frac{m_2}{m_0}}, \quad m_i = \int_0^{\infty} n^i S_y(n) dn, \quad h_3 = \frac{\gamma_3}{4 + 2\sqrt{1 + 1.5\gamma_4}}, \\ h_4 = \frac{\sqrt{1 + 1.5\gamma_4} - 1}{18}, \quad \kappa = \frac{1}{\sqrt{1 + 2h_3^2 + 6h_4^2}} \end{gathered} \tag{3}$$

where ν_0 is the mean zero up crossing rate of process y (standardized non-Gaussian process obtained from a non-Gaussian process x, $y = (x - E[x])/\sigma_x$), T is the duration, m_i is the i^{th} spectral moment of y, $S_y(n)$ is the one-sided power spectral density of y, n is the frequency in Hz. The validity range of the application of Hermite model is defined in a monotonic region, *i.e.* corresponding to a monotone transformation of *x(u)*, requiring *dx/du > 0*. Practically, this condition satisfies [7, 14],

$$\gamma_e \geq (1.25\gamma_3)^2 \tag{4}$$

Choi [21] studied the different regions and monotone limits of Hermite-based model (for softening and hardening processes). Strong negative wind pressures measured on buildings and roofs are mostly softening processes. In our case, taps falling outside the monotone limit are in region III of Figure 1(a). Choi [21] proposes to overcome this limit by taking a softening-hardening-softening transformation (Figure 1(b)) in order to keep an increasing (monotone) transformation *x(u)* and cross the decreasing part of the softening process. This technique requires making a hybrid model depending on the value of x and deform the nature of the process.

Another methodology to deal with these processes is proposed in the next section, based on physical interpretation in the case of bimodal processes.

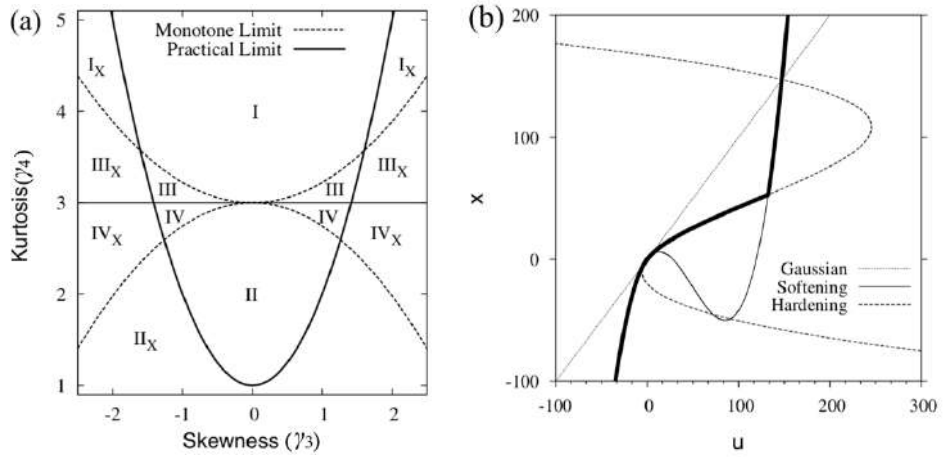

Figure 1. (a) Regions of Hermite model applicability, (b) Region III of Figure 1a: softening-hardening-softening truncation for monotone transformation *x(u)* (Choi (2010)).

2.2 *Autocorrelation-aided de-mixing algorithm*

Pressure processes in the corner vortices region are highly non-Gaussian and bimodal. Based on this physical interpretation, instead of using the whole PDF in a non-monotone transformation, we propose to use only the mode of interest in the cubic model: the one containing the tail. Each PDF has thus first to be decomposed.

Cook [20] proposed to model the wind pressure data as a sum of several components, the Skew Gaussian Exponential Mixture Model (SGEMM). Inspired by this model, we suggest modeling the wind pressure as a mixture of two skew-Gaussian (SG) distributions. The skew-gaussian (SG) is given by

$$p_{SG}(x) = 2\phi\left(\frac{x-\xi}{\omega}\right)\Phi\left(\alpha\frac{x-\xi}{\omega}\right) \tag{5}$$

where ϕ and Φ are the standard gaussian PDF and cumulative density distribution (CDF), ξ a location parameter, ω a scale parameter and α a skewness parameter. It is also possible to use another distribution, the skew-hyperbolic secant, to fit only the tail but we keep only two SG distributions thanks to the physical interpretation: (i) mode 1 corresponding to the turbulent background flow (as the one present on the roof region without vortex) and (ii) mode 2 to the corner vortices fluctuation (separated flow). The resulting PDF is the weighted combination of those distributions,

$$P(x) = w_1 p_1(x) + w_2 p_2(x) \tag{6}$$

where w_i are weighted parameters. Standard adjustment methods would recommend proceeding to a non-linear least-squares fitting to find appropriate estimates of 8 model parameters, under the constraint $w_1 + w_2 = 1$. In the case of a bi-modal PDF, the mean and the variance of the total PDF can be linked to those of its components 1 and 2,

$$\mu = w_1\mu_1 + w_2\mu_2, \text{ with } w_1 + w_2 = 1 \tag{7}$$

$$\sigma^2 = w_1\sigma_1^2 + w_2\sigma_2^2 + w_1 w_2 (\mu_1 - \mu_2)^2 \tag{8}$$

When bumps are clearly identifiable, initial guesses for the location and scale parameters (ξ, ω) are easy to choose and the fitting converges quickly

2.3 *Slow and fast time scales*

Standard adjustment methods work well when the modes are easy to identify but can be ill-conditioned in some limit cases (e.g. same average and/or standard deviation for two modes). In this case, a more robust method is necessary. The idea comes from a physical interpretation of the modes from a timescale point of view. Close to edges of buildings, two phenomena are involved in the pressure, a mixture between a slow background turbulence (mode 1) and a fast shedding (mode 2), which is visible in the autocorrelation function of the mixed process, expressed as,

$$R(t_1,t_2) = \int_{-\infty}^{+\infty} (x_1-\mu)(x_2-\mu) P_x(x_1,x_2,t_1,t_2)\,\mathrm{d}x_1\mathrm{d}x_2 \tag{9}$$

where $P_x(x_1,x_2,t_1,t_2)$ is the probability to have the pressure coefficient $x=x_1$ at t_1 and $x=x_2$ at t_2. In a mixture model, the random variable is either in mode 1 or mode 2. The pressure coefficient can be represented by,

$$c_p(t) = w_1(t)c_{p,1}(t) + w_2(t)c_{p,2}(t), \text{ with } c_p = \frac{p-p_\infty}{\frac{1}{2}\rho U_\infty^2} \tag{10}$$

where $w_i(t) = 1$ if c_p is in mode 1, and 0 otherwise. The weight has thus also a certain dynamics, and probability distribution $P_{w_1}(i,j,t_1,t_2)$ where i at time t_1 and j at time t_2 are equal to 0 or 1. We have $P_{w_1}(1,0,t_1,t_2) = P_{w_2}(0,1,t_1,t_2)$. The signal being stationary, we can rewrite the autocorrelation depending on $\tau = t_1 - t_2$,

$$\begin{aligned} R(\tau) = \quad & P_{w_1}(1,1,\tau)R_1(\tau) + P_{w_1}(0,0,\tau)R_2(\tau) + P_{w_1}(1,1,\tau)\left(\mu_1^2 - 2\mu\mu_1\right) + P_{w_1}(0,0,\tau)\left(\mu_2^2 - 2\mu\mu_2\right) \\ & + 2P_{w_1}(1,0,\tau)\left(\mu_1\mu_2 - \mu\left(\mu_1+\mu_2\right)\right) + \mu^2 \end{aligned} \tag{11}$$

The general expression of the autocorrelation is thus based on the sum of two decreasing exponentials, the autocorrelation of each mode,

$$R_i(\tau) = \sigma_i^2 e^{-\tau/\tau_i} \tag{12}$$

where τ_i is the characteristic time of mode *i (i = 1,2)*. Two limit cases are interesting to analyze:

$$\lim_{\tau\to 0} R(\tau) = \overline{w}_1 R_1(0) + \overline{w}_2 R_2(0) + \overline{w}_1\overline{w}_2\left(\mu_1-\mu_2\right)^2 \tag{13}$$

where $\overline{w}_i$ is the mean of $w_i(t)$. Equation 13 is consistent with Equation 8.

$$\lim_{\tau\to\infty} R(\tau) = \overline{w}_1^2 R_1(\tau\to\infty) + \overline{w}_2^2 R_2(\tau\to\infty) = 0 \tag{14}$$

When the mean pressures in both modes are close to each other (standard methods are ill-conditioned), the third term in Equation 13 is negligible and by identifying the two components in the autocorrelation function, it is possible to extract the weighted variance of each mode and use them as an additional constraint in the fitting. Figure 2 summarizes the autocorrelation-aided de-mixing methodology in two modes.

One the bi-modal distribution is properly de-mixed, the peak factor estimation is performed using the model of Kareem and Zhao [4] on Mode 2 only (the one associated to the most negative pressures).

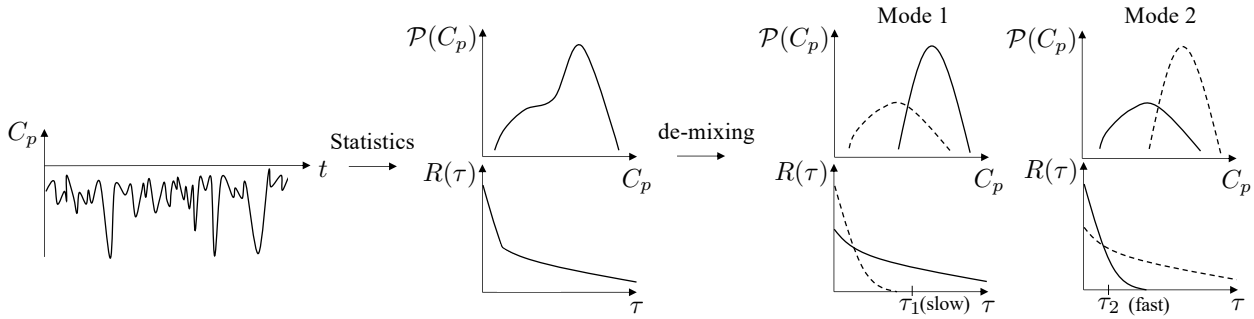

Figure 2. Autocorrelation-aided de-mixing methodology.

3 CASE STUDY

The setup made by Blaise *et al.* [16] consists of a square plan-form low-rise building (sides of 45 m and a height of 25 m), uniformly instrumented by 121 pressure taps in a quarter of its roof (see Figures 1 and 2), sampled at $f_s = 500$ Hz. The model is placed at an incidence of 45° in the atmospheric boundary layer test section of the wind tunnel (WT) of the University of Liege. This direction is fixed to obtain a symmetry in the complex nature of the corner vortices developed at the edges [17].

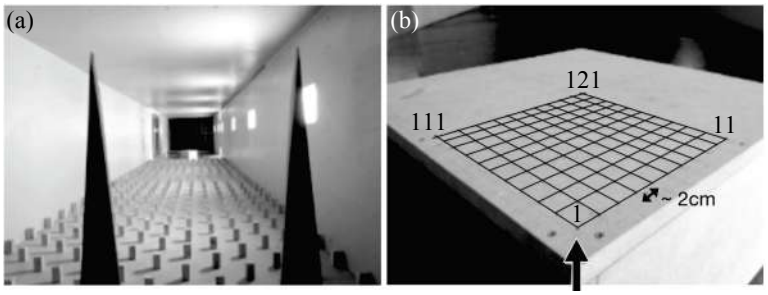

Figure 3. (a) Model inside the WT, (b) location of pressure taps on the model (wind direction fixed at 45°).

The atmospheric boundary layer test section creates a turbulent wind of category III according to the Eurocode [18], with $z_0 = 0.3$ m and $z_{min} = 0.5$ m. The mean velocity (Equation (15)) and turbulence intensity (Equation (16)) profiles are presented in Figure 4.

$$U_\infty(z) = U_{ref} k_r \ln(z/z_0), k_r = 0.19(20z_0)^{0.07} \tag{15}$$

$$I_u(z) = \frac{1}{\ln\left(\frac{z}{z_0}\right)} \tag{16}$$

Pressure taps are linked to the scanner using pneumatic connection (vinyl tubes) of internal diameter of 1.32 mm and length 600 mm. The static pressure is well measured but unsteady components have to be dynamically corrected, thanks to the theoretical formulation of Bergh and Tijdeman [19] and the experimental apparatus of Rigo [20]. Figure 5 presents the transfer function, in amplitude and phase, necessary to correct measurements, until the sampling frequency of 500 Hz.

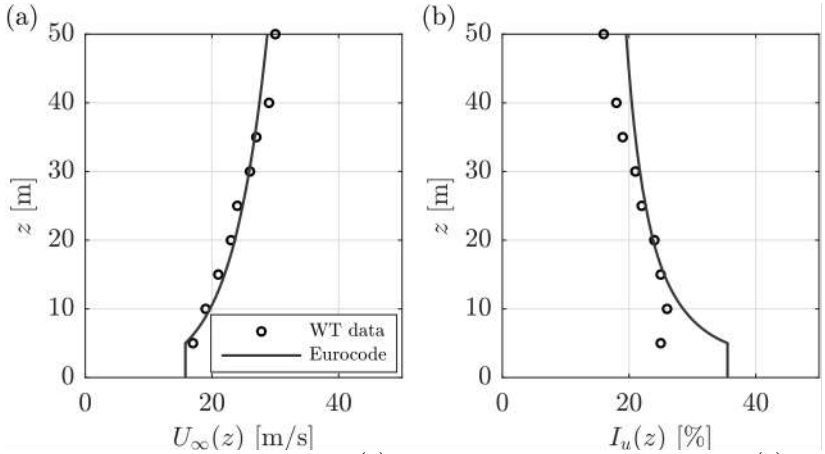

Figure 4. (a) Mean velocity $U_\infty(z)$ and (b) turbulence intensity $U_\infty(z)$ profiles of the atmospheric boundary layer: measurements and comparison with suburban category III terrain, from [16, 18].

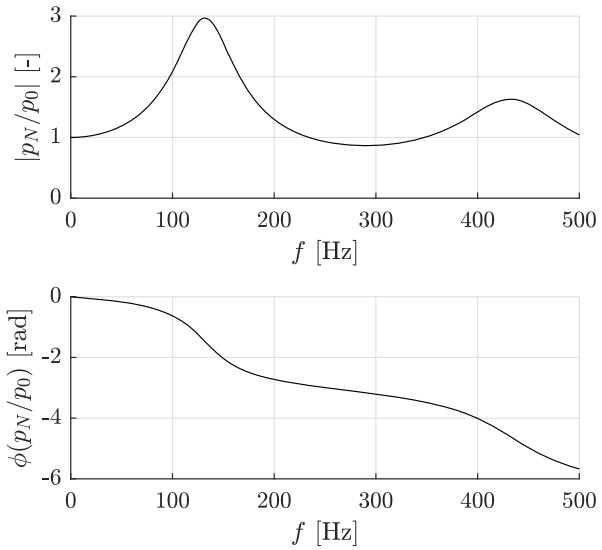

Figure 5. Transfer function of the pressure tubes, in amplitude and phase of corrected pressure as a function of the frequency [19, 20].

3.1 *WT results: First rank statistics*

The geometric scaling is $\lambda_L = 1/100$. The Reynolds condition would require a velocity scaling of $\lambda_U = \lambda_L^{-1} = 100$, which would impose WT speed of about 1000 m/s, impossible. The Reynolds dependency is more critical for smooth and mainly circular shapes such as cylinder or sphere. When the flow is completely separated and turbulent, the Strouhal scaling is preferred. Because of WT performances, the velocity scaling is chosen as $\lambda_U = 1/3.5$. The Strouhal condition imposes $\lambda_T = \lambda_L/\lambda_U = 1/28.6$ (time). Every measurement is converted in full scale. A total of 13 h of measurement has been taken in the WT, corresponding to 371.8 h full scale. This long information allows to compute precise PDF tail, necessary to study the extreme values. In the following, statistics are presented in a non-dimensional way: position $(\xi, \eta) = (x/L, y/L)$ and pressure coefficient (Equation (10)).

The Reynolds number of the WT model is 6.8×10^5. The flow around this low-rise building is characterized by corner vortices, that roll in a cone shape. The pressure is mainly negative because of the separated nature of the flow ($\mu(C_p)$ in Figure 6(a)) and is the most negative where it starts to separate, just after the edges, on the corner. The two cones on both corners have a main

axis, recognizable by the ridgelines of the standard deviation of the pressure coefficient $\sigma(C_p)$, in Figure 6(b). The non-Gaussianity happens in the corner vortices boundaries, where $\gamma_3(C_p)$ and $\gamma_e(C_p)$ are the highest. For a Gaussian process, $\gamma_3 = 0$ and $\gamma_4 = 3$. The excess $\gamma_e = \gamma_4 - 3 = 0$. On Figure 6, a lower right triangle appears systematically, with low statistics values. This region is mainly Gaussian, with a low dispersion and mean pressure value. Physically, the flow in this region is the case of a simple turbulent flow on a flat plate. This region is not studied here, since it has smaller extreme values and represents less interest compared to the complex flow in corner vortices.

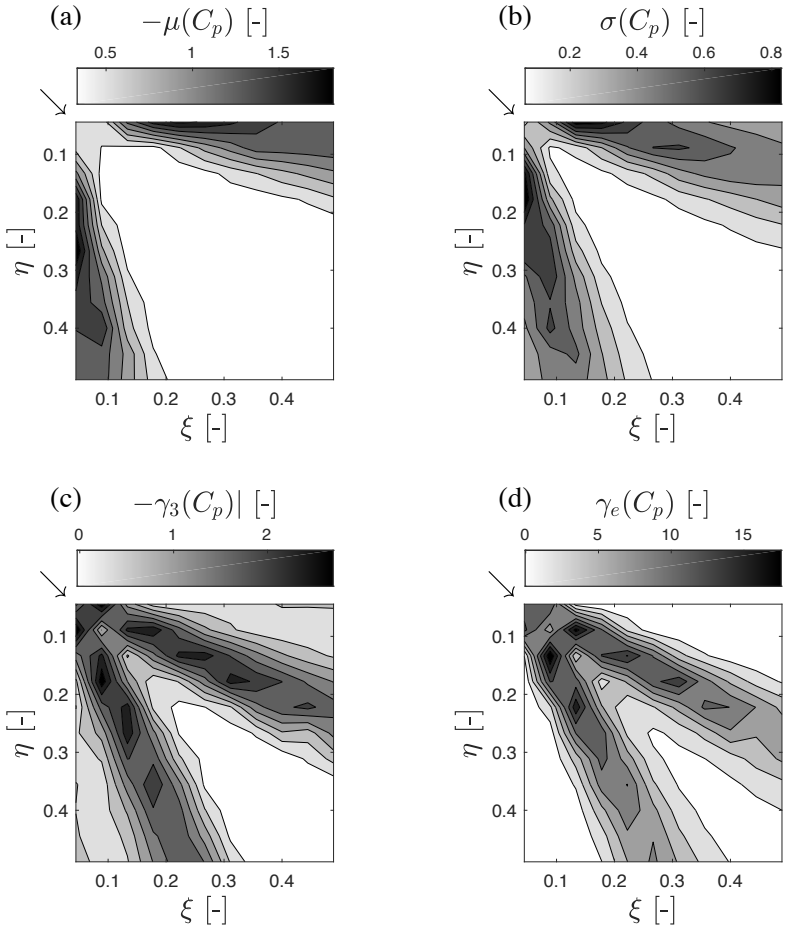

Figure 6. Map of (a) mean, (b) standard deviation, (c) skewness and (d) kurtosis (excess).

As suggested by Kawai [14], there is one main vortex at the corner, but a secondary small one develops just next to the edge, below the main vortex. Pressure taps in this setup were not close enough to the edge to capture well this secondary vortex. Nevertheless, in Figure 6, $\gamma_3(C_p)$ increases just next to the edge, at $(\xi, \eta) = (0.05, 0.4)$, suggesting the presence of another vortex. By looking at skewness and kurtosis values, each pressure distribution in the corner vortices has a negative skewness (negative extreme pressure events) and a positive excess kurtosis (called softening process, the PDF has a flatter shape compared to a Gaussian process). Figure 7 shows a typical pressure coefficient signal (at tap 4): with local negative extreme pressures ($\gamma_3 < 0$) and wide range of distributed values, no concentrated values around the mean. Moreover, the two modes are identifiable with two principal levels at around $c_p = -0.9$ and -2.1.

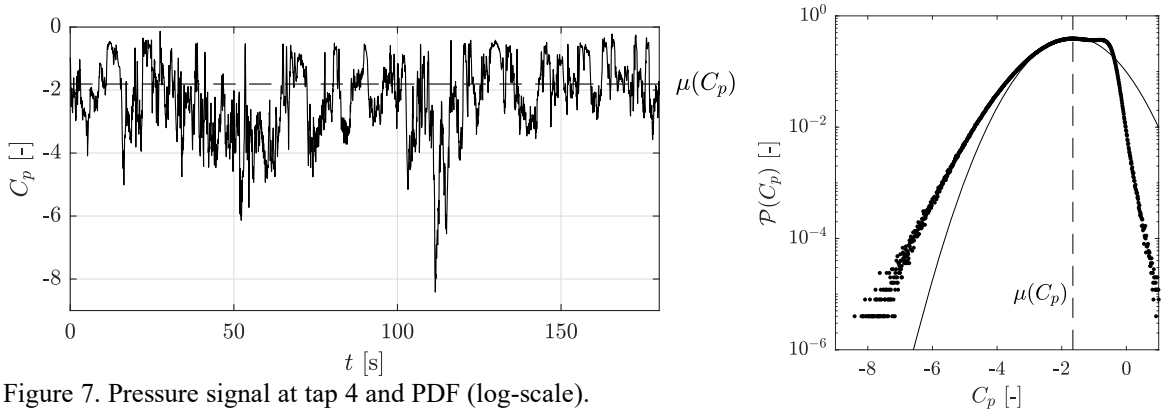

Figure 7. Pressure signal at tap 4 and PDF (log-scale).

Figure 8 allows to have a quick qualitative view of the PDF. Each PDF is represented in log-scale at all 121 pressure tap locations. The same scaling is used to represent them and have a quick comparative view of the dispersion and asymmetry of PDFs. Those in the corner vortices are highly non-Gaussian and two modes (two bumps) are clearly identifiable. This motivates the discussion of Section 4.

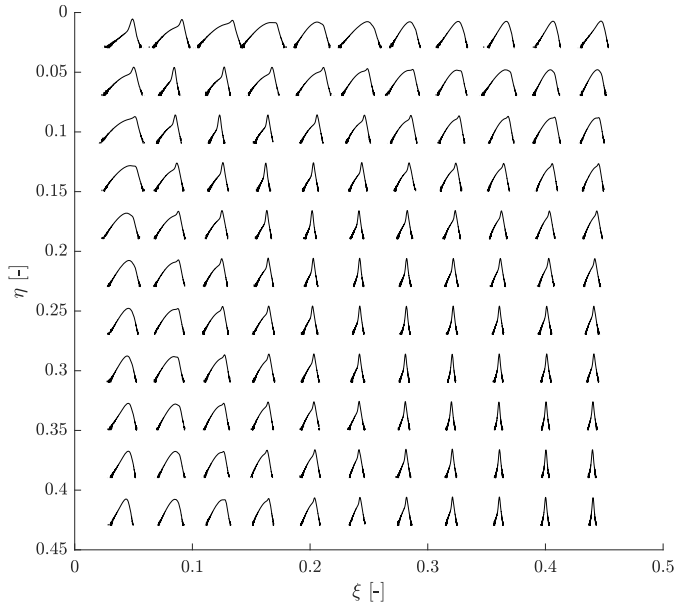

Figure 8. Map of all PDFs.

3.2 *Extreme values*

As done for the pressure coefficient signal, it is also possible to compute statistics and draw probability density functions for peak pressures. Based on time series, the peak value of cp over a time window T (conventionally 10 min full-scale) is taken. This operation is repeated for the whole signal so that the peak pressure is not unique and has a distribution. Figure 9 shows PDF of extreme pressures for taps 56 to 60, which cross the corner vortices region: (i) close to the edge (56), the pressure is significantly negative, (ii) in the corner vortices region (from tap 57 to 59), the extreme distribution is wider, (iii) after the corner vortices, where only background turbulence remains, the peak pressure is less negative and its distribution quite narrow.

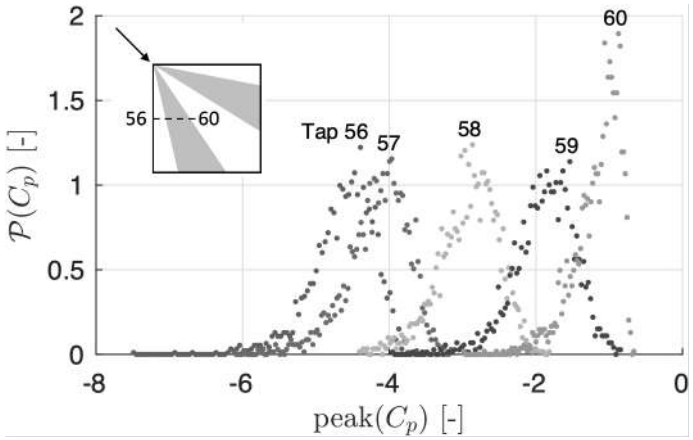

Figure 9. PDF of peak pressures (10 min window) of taps inside corner vortices region.

Figure 10(a) shows a map of the mean value of peak factor of the pressure coefficient $\mu_g(C_p)$, the highest values happening were the vortex cone touches the roof, similarly to γ_3 and γ_e.

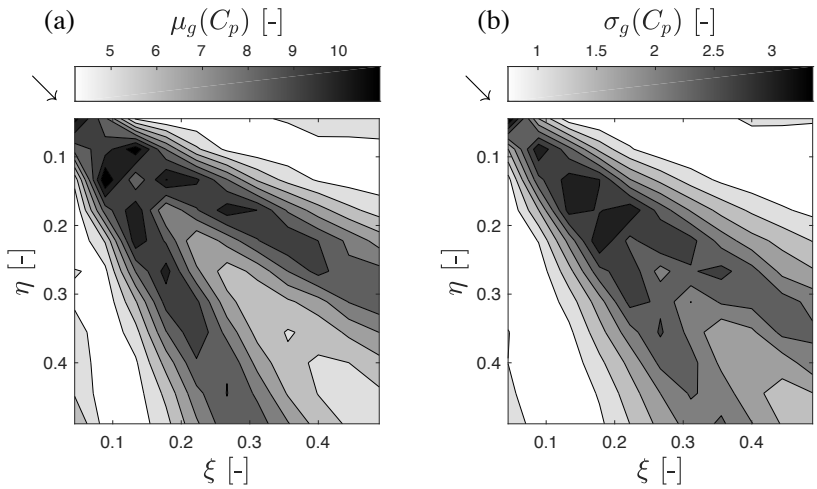

Figure 10. Map of peak factor (a) mean and (b) standard deviation.

4 RESULTS AND APPLICATIONS

4.1 *De-mixing algorithm*

Figure 11 shows the decomposition in modes of the PDF at pressure tap 4. The two modes are easy to identify by looking at the two bumps in the PDF (Figure 11(a)). Figure 11(b) show that the de-mixing algorithm and modes identification is not susceptible to the duration of measurement, only the tail is limited to probability of 10^{-4}. While the computation of peak factor directly from data requires long measurements, the peak factor estimation from de-mixing is quicker.

Figure 12(a) show the PDF at tap 11, modes are almost superimposed and less easy to identify. The autocorrelation (Figure 12(b)) is decomposed in two modes and the weighted variance of each mode is extracted from the value at the origin to constrain the PDF fitting.

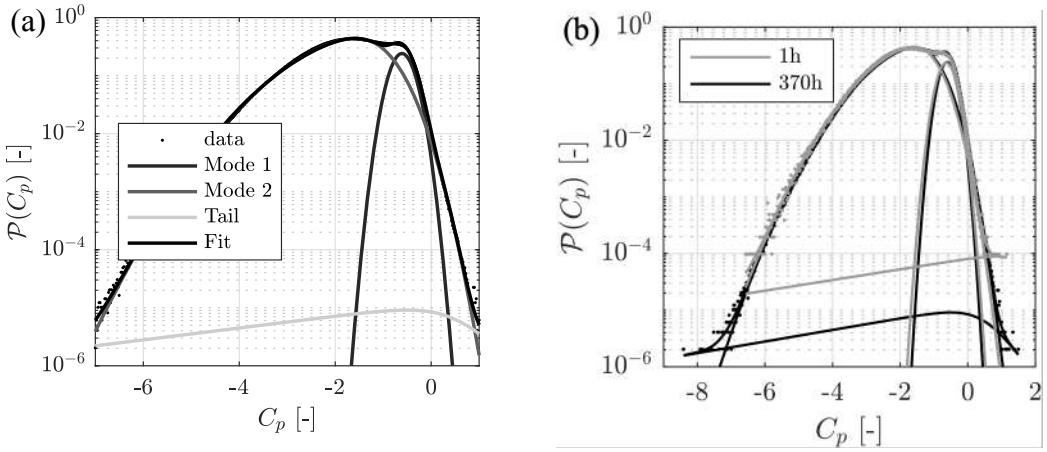

Figure 11. Tap 4: (a) PDF decomposition in mode 1, 2, tail (log-scale) and (b) influence of duration measurement.

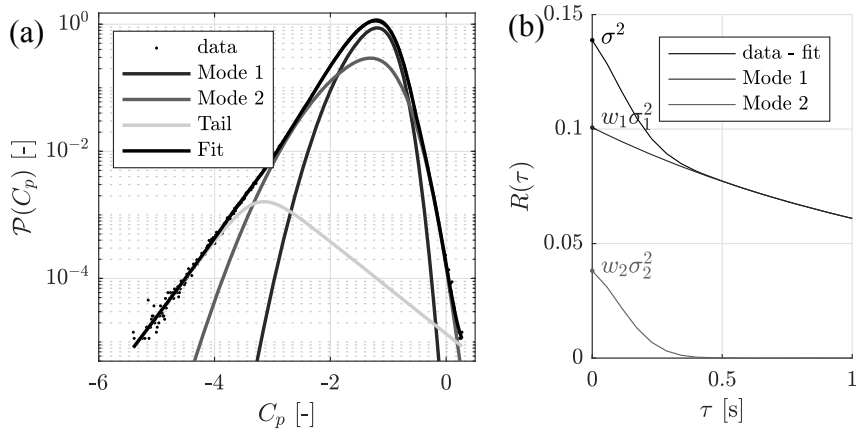

Figure 12. Tap 11: (a) PDF decomposition in mode 1, 2, tail (log-scale) and (c) autocorrelation decomposition in modes 1 and 2.

4.2 *Extreme values estimation*

Figure 13 compares results (a) before and (b) after de-mixing. The boundary of Equation (4) is shown in Figure 13(a), where pressure taps belonging to the lower region are not eligible (without de-mixing). These taps a represented on the right in Figure 13(a), precisely in the corner vortices region. The taps outside the monotone limit (before de-mixing) are used in the de-mixing methodology and the skewness-kurtosis map of each mode is reproduced. The monotone criterion is fulfilled for all taps after de-mixing: (i) Mode 1 represents the background turbulence and is almost Gaussian (low γ_3 and γ_e) while (ii) Mode 2 associated to corner vortices and peak pressure is more non-Gaussian but still inside the monotone region. Figure 13(c) shows the peak factor estimation compared to the measured one without and with de-mixing. Thanks to the decomposition, the statistics used from mode 2 allows to satisfy the monotone limit and improve the peak factor estimation.

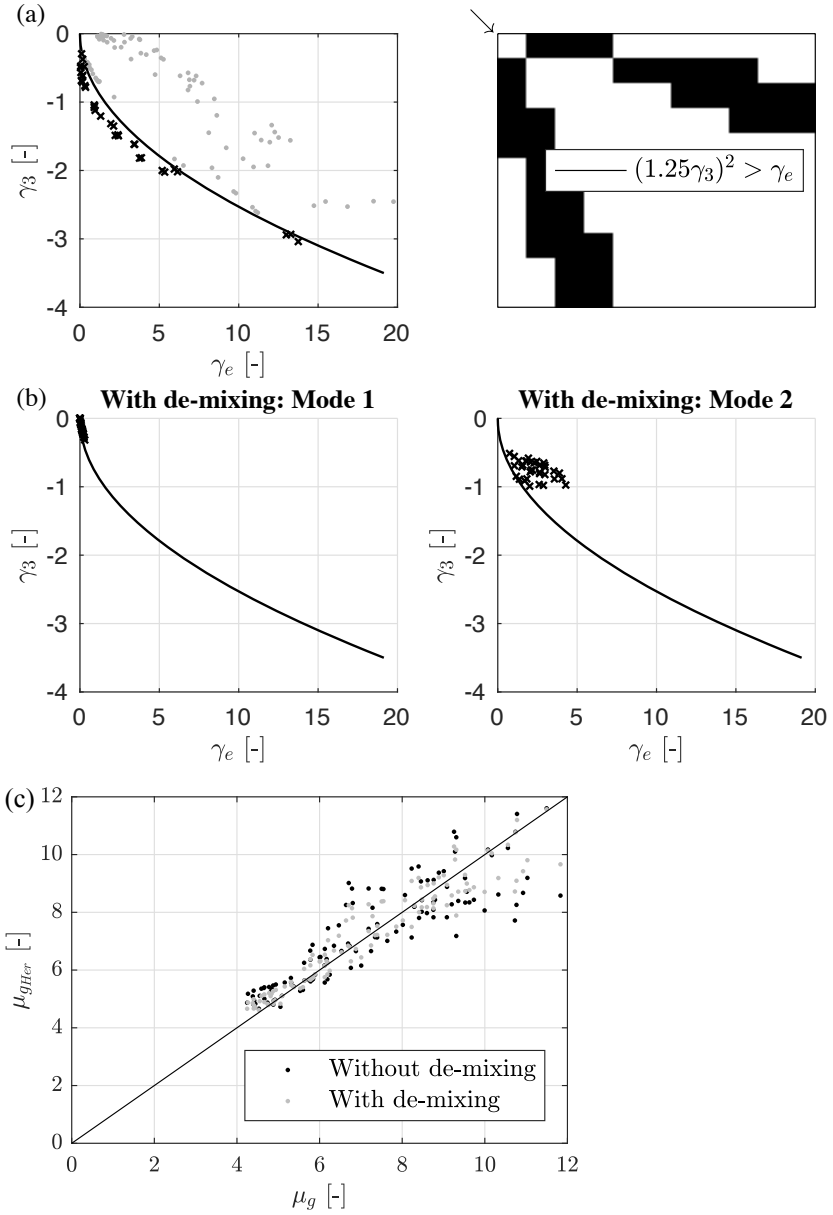

Figure 13. De-mixing methodology results: (a) skewness-kurtosis monotone region (a) before de-mixing (• taps inside the limit and × outside, and location on the roof) and (b) after de-mixing of taps that were outside in (a) for the two modes, (c) peak factor estimation improvement.

4.3 *Dynamic response of a cladding*

In structural design, the peak pressure is usually statically applied on the whole cladding surface. Often, this leads to a too conservative design because the façade element response might react in a dynamic manner to fast loadings. Indeed, a very large negative peak occurring during a very short period of time will less affect the structure (depending on its natural frequency); the severity of such an impulsive load depends on its momentum (dashed part of the time signal in Figure 14). The dynamic response is computed by applying the pressure excitation on a simple mass-spring-damper system. The response spectrum is sketched in Figure 14 (right) by reporting the ratio between the maximum dynamic response over the maximum static one for each natural frequency (by varying its stiffness). When the PDF is bimodal, the shock response spectrum pre-

sents also an envelope with two modes: the slow turbulent background (high characteristic time, low frequency) and the fast shedding (lower time, higher frequency). Thanks to the decomposition, the response in each mode can be estimated very efficiently: momentum for the fast vortices and power spectral density for the turbulence.

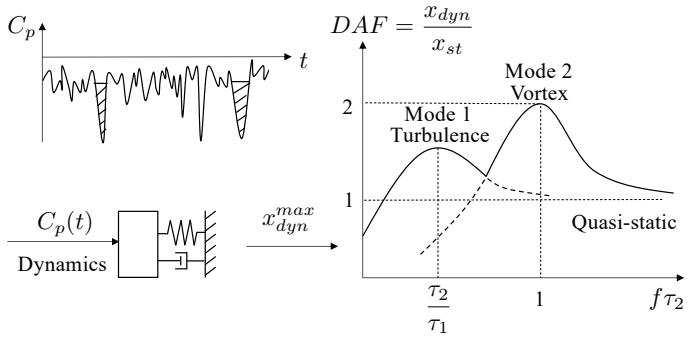

Figure 14. Dynamic response of a cladding and shock response function.

5 CONCLUSIONS

In conclusion, in order to correct peak factor estimations based on cubic translation model, strong non-Gaussian pressure processes that are not inside the monotonic region have been corrected by decomposing their PDF into two competing sources of wind pressure, associated to different known physical phenomena : (1) the fast shedding in separated regions (corner vortices) and (2) the slow background turbulence. Mode 2 is responsible for large negative peaks and is therefore the relevant one to estimate peak factors using Hermite moment-based model. Doing so provides a much better agreement with long time series.

6 ACKNOWLEDGEMENTS

The authors want to thank the Belgian National Fund for Scientific Research (FNRS) for their support.

7 REFERENCES

1 N.J. Cook. On the gaussian-exponential mixture model for pressure coefficients. 153:71–77, 06, 2016.
2 L. Amerio, A. Allsop, G. Pomaranzi, and A. Zasso. Experimental assessment of the current techniques for the assessment of the area- averaged wind-pressure using wind tunnel pressure data. In Proceedings of the UK Wind Engineering Society Conference, Leeds, UK, 2018.
3 L-X. Lin, D. Surry, and H.W. Tieleman. The distribution of pressure near roof corners of flat roof low buildings J. Wind Eng. Ind. Aerodyn. 56 235-265, 1995.
4 Kareem, A., and Zhao, J., Analysis of non-Gaussian surge response of tension leg platforms under wind loads, J. offshore Mech. and Arctic Eng., ASME, 116, 137-144, 1994.
5 Sadek, F., and Simiu, E., Peak non-Gaussian wind effects for database-assisted low-rise building design, J. Eng. Mech., ASCE, 128(5), 530-539, 2002.
6 Chen, X. and Huang, G., Evaluation of peak resultant response for wind-excited tall buildings. Engineering Structures 31, 858-868, 2009.
7 Kwon, D.K. and Kareem, A., Peak Factors for Non-Gaussian Load Effects Revisited, J. Struct. Eng., 137(12): 1611-1619, 2011.

8 Huang, M., Huang, S., Feng, H., Lou, W., Non-Gaussian time-dependent statistics of wind pressure processes on a roof structure. Wind and Structures an International Journal. 23. 275-300. 2016.
9 Grigoriu, M., Crossings of non-Gaussian translation processes, J. Eng. Mech., ASCE, 110(4), 610-620, 1984.
10 Winterstein, S.R., Moment-based Hermite models of random vibration, Lyngby, Report No. 219. Department of Structural Engineering, Technical University of Denmark, Lyngby, Denmark, 1987.
11 Davenport, A. G., Note on the distribution of the largest value of a random function with application to gust loading, J. Inst. Civ. Eng., 24, 187-196, 1964.
12 Tognarelli, M. A., Zhao, J., and Kareem, A., Equivalent statistical cubicization for system and forcing nonlinearities, J. Eng. Mech., ASCE, 123(8), 1772-1790, 1997.
13 Winterstein, S. R., Ude, T. C., and Kleiven, G., Springing and slow-drift responses: predicted extremes and fatigue vs. simulation, Proc. BOSS-94, 3, MIT, 1-15, 1994.
14 Winterstein, S.R. and MacKenzie, C.A., Extremes of nonlinear vibration: models based on moments, L-moments, and maximum entropy, J.Offshore.Mech. Arct., 135(2), 021602, 2012.
15 Peng, X., Luping Yang, L., Gavanski, E., Gurley, K. and Prevatt, D., A comparison of methods to estimate peak wind loads on buildings, J. Wind Eng. Ind. Aerodyn., 126, 11–23, 2014.
16 Blaise, N., Andrianne, T., and Denoël, V., Assessment of extreme value overestimations with equivalent static wind loads, J. of Wind Engineering and Industrial Aerodynamics 168, 123– 133, 2017.
17 Kawai, H., Nishimura, G., Characteristics of fluctuating suction and conical vortices on a flat roof in oblique flow, J. Wind Eng. Indus. Aerodyn. 60, 211–225, 1996.
18 Eurocode, E., EN 1991-1-3: Actions on Structures-General Actions-Wind Actions. European Committee for Standardization, 1991.
19 Berg, H., Tijdeman, H., Theoretical and experimental results for the dynamic response of pressure measuring systems. National Aero and Aeronautical Research Institute, NLR-TR F.238, 1965.
20 Rigo, F., Unsteady pressure measurement around aerodynamic bodies: Development of a calibration apparatus and wind tunnel testing. Master's dissertation, University of Liège, 2017.
21 Choi, M. and Sweetman, B., The Hermite Moment Model for Highly Skewed Response with Application to Tension Leg Platforms, ASCE Journal of Offshore Mechanics and Arctic Engineering, 132, Issue 2, 2010.